Chapter 10 The Ozone Layer

10.1 Introduction

It has been known for more than 50 years that ozone in the atmosphere is largely confined to the stratosphere, with the maximum molecular concentration occurring near 22 km and the maximum mixing ratio near 35 km (see Figs. 1.6 and 1.7). Ozone, by its absorption of solar radiation of wavelengths less than 300 nm, provides the heat source that is responsible for the global mean increase of temperature between the tropopause and the stratopause; in the absence of ozone there would be no stratosphere! The ozone layer, through its absorption of harmful ultraviolet radiation, is also essential for the health of plant and animal life. Thus, study of the formation, maintenance, and stability of the ozone layer is a critical aspect of middle atmosphere science.

Chapman (1930) formulated the first plausible model for the existence and vertical structure of the ozone layer. The Chapman mechanism begins with the photolysis of O_2 by solar ultraviolet radiation of wavelengths less than 250 nm (see Section 2.3.1). The atomic oxygen thus produced combines with ground-state molecular oxygen to form ozone. The amount of shortwave radiation available for photodissociation of O_2 decreases downward from the top of the atmosphere, with the most rapid rate of decrease occurring at high latitudes where the optical path is long [see Eq. (2.2.16)]. Since the amount of O_2 available for reaction with atomic oxygen decreases exponentially away from the earth's surface, the production of ozone must be a maximum in a layer (sometimes called the Chapman layer; see Section 2.7) centered in low latitudes at some intermediate altitude. Chapman proposed that photochemical production of ozone was balanced by destruc-

tion through the reaction of ozone with atomic oxygen. His scheme is now known to be a very incomplete model of ozone layer photochemistry (see Section 10.4). Nevertheless, it provides a useful conceptual model.

Although the existence of ozone depends on photochemical reactions, its distribution in the atmosphere can only be explained by taking account of the role of atmospheric motions in transporting ozone from its source region in the tropical upper stratosphere to the high-latitude lower stratosphere where it behaves as a quasi-conservative tracer. The motions responsible for this transport are strongly influenced by the heating distribution associated with solar absorption in the ozone layer. Thus, it is necessary to consider the three-way interactions among chemistry, radiation, and dynamics in order to understand the distribution and temporal variations of ozone.

10.2 The Climatology of Ozone

There is a long history of ozone observations from ground-based instruments, balloons, rockets, and satellites. Ground-based measurements make use of the fact that the absorption of solar radiation by ozone is highly wavelength-dependent. Thus, comparison of the atmospheric absorption in several wavelength regions makes it possible to deduce the total column of ozone. Similar measurements can be made from satellites by observing the ultraviolet radiation backscattered from the surface and clouds. Ozone also absorbs in the infrared, so that total ozone can be deduced from space by measuring the total extinction of upwelling thermal infrared radiation in appropriate wavelength bands.

10.2.1 Total Ozone

The total column abundance of ozone determines the amount of radiation that can reach the surface of the earth in the near-ultraviolet region (290–310 nm), and hence the potential for damage to the biosphere. Total ozone is usually expressed in terms of the equivalent thickness of the ozone layer at standard temperature and pressure (STP; 0°C, 1013.25 mb). This thickness is about 3 mm (STP) for a column containing the global mean amount of ozone (8×10^{22} molecules m^{-2}). Maps of the distribution of total ozone often have the column abundance expressed in terms of Dobson units (DU), where 1 DU = 10^{-5} m (STP). Thus, the global mean total ozone is about 300 DU.

A 4-year average total ozone map based on data from the TOMS satellite backscatter ultraviolet instrument on *Nimbus* 7 is shown in Fig. 10.1. There is a general increase of total ozone from equator to high latitudes in both hemispheres, but with larger amounts in the Northern Hemisphere. Although longitudinal variations are fairly small in this long-term average, there are on average distinct maxima in midlatitudes over the east coasts of Asia and North America and over Eastern Europe during winter, corresponding to the mean positions of the troughs in the stationary planetary-wave pattern of the upper troposphere.

The seasonal variation of the zonal-mean total ozone field derived from the TOMS data is shown in Fig. 10.2. There is a large-amplitude annual cycle in the extratropical regions of both hemispheres, but with a substantially larger range in the Northern Hemisphere. Maxima occur just after the spring equinox near 90°N and 60°S; a minimum occurs near 90°S (the Antarctic ozone hole).

Although the time mean and seasonal variability of the total ozone field primarily depend on latitude, longitudinal variations in total ozone can be quite large on individual days. Since most of the ozone molecules in a column are confined to the lower stratosphere, the synoptic pattern of total ozone reflects the variations in tropopause height associated with tropospheric disturbances. In particular, total ozone tends to be highest on the cyclonic side of upper level jetstreams (see Section 9.6.1) and in the region of isolated cyclonic vortices (cutoff lows). Thus, to some extent total ozone is a tracer for large-scale meteorological processes in the upper troposphere.

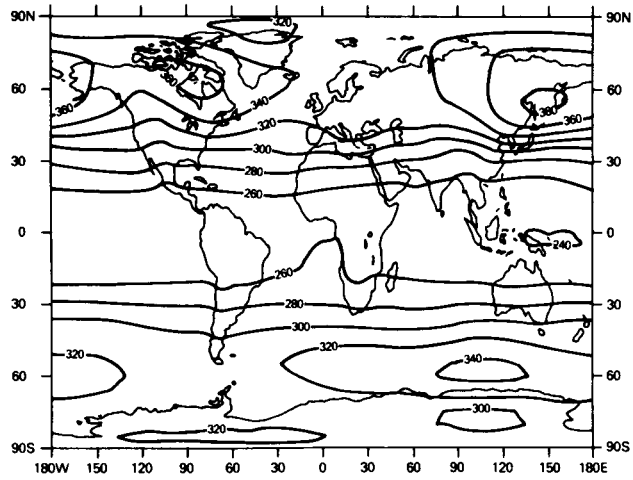

Fig. 10.1. Global distribution of total ozone (Dobson units) based on 4 years of observation with the TOMS instrument on the *Nimbus* 7 satellite. [After Bowman and Krueger (1985).]

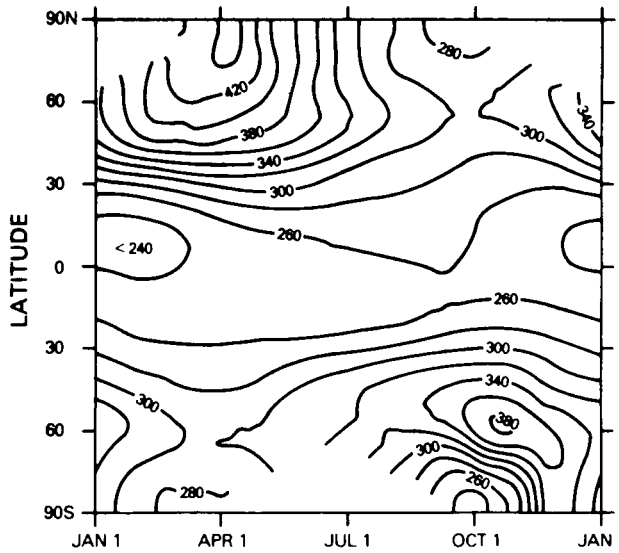

Fig. 10.2. Time-latitude section showing the seasonal variation of total ozone (Dobson units) based on TOMS data. Note the springtime maxima near 90°N and 60°S and the minimum near 90°S. [After Bowman and Krueger (1985).]

10.2.2 The Vertical Distribution

The vertical distribution of ozone in the troposphere and stratosphere up to about the 10-mb level has been observed *in situ* by balloon-borne ozonesondes. Above the 10-mb level, limited *in situ* measurements are available from rockets. These balloon and rocket data have been used to establish the standard profiles shown in Figs. 1.6 and 1.7. Recently satellite observations on *Nimbus* 7 and the Solar Mesosphere Explorer (SME) satellites have provided global measurements of the ozone distribution in both the stratosphere and the mesosphere.

Before discussing the observed distribution, it is useful to consider the various conventions used in presenting ozone data. Ozonesonde profile data are usually plotted in terms of the partial pressure of ozone in nanobars (nb). The mass mixing ratio and the volume mixing ratio given by Eq. (1.3.3) are also in common use. For ozone these are expressed in parts per million by mass (ppmm) and parts per million by volume (ppmv), respectively. Satellite data are usually expressed in ppmv. Recall from Eq. (1.3.3) that the volume mixing ratio is equal to the partial pressure of ozone divided by the air pressure. Also, note that the volume mixing ratio for ozone is about 0.6 times the mass mixing ratio. By contrast, chemical equations [e.g.,

Eq. (10.3.2) or Eq. (10.3.3)] are usually expressed in terms of the number density.

An example of a single ozonesonde profile was given in Fig. 9.7, where ozone was plotted with partial pressure on the abscissa but was labeled by the contours of mass mixing ratio (curves sloping downward toward the right). The fine vertical-scale structure in the ozone sounding of Fig. 9.7 is quite common in individual observations of ozone (and other quasi-conserved tracers). Such variability is of course averaged out in long-term averages such as the monthly mean curves given for a polar station (Resolute,

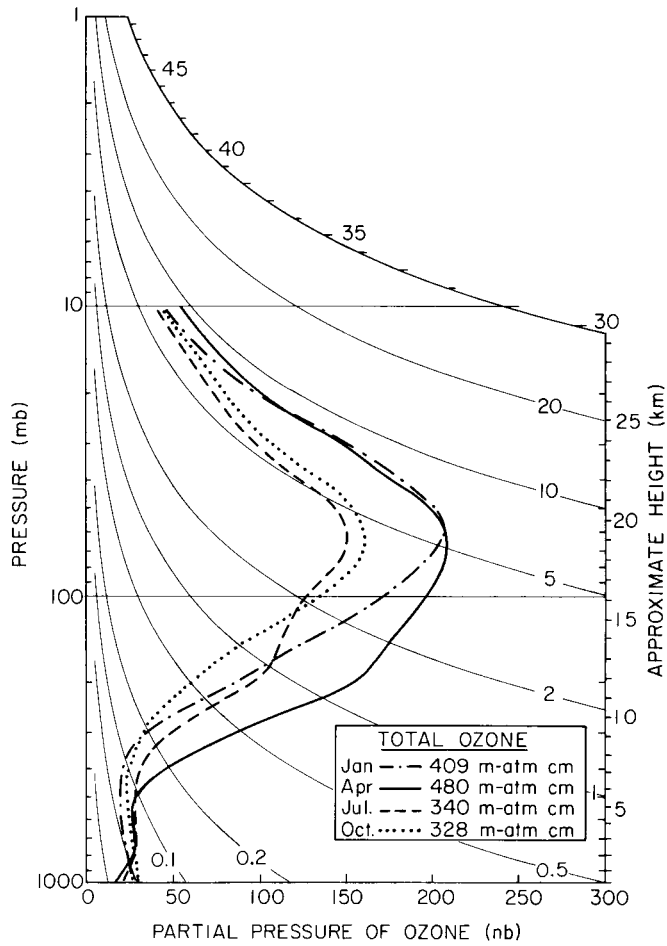

Fig. 10.3. Vertical profiles of ozone for four seasons at a polar station (Resolute, 75°N). Lines curving downward toward the right are isolines of constant mixing ratio (ppmv). [Courtesy of Professor J. London. Adapted from London (1985).]

75°N) in Fig. 10.3. As this figure shows, the spring maximum in total ozone that was discussed earlier is largely accounted for by the seasonal variation of the ozone concentration in the 50- to 100-mb height range (where the maximum concentration lies); above 50 mb the mixing ratio actually decreases slightly from January to April, while below 300 mb there is a small decrease from October to January.

Satellite observations over the past 20 years have provided a global climatology of ozone mixing ratio in the stratosphere and mesosphere. In most cases the satellite data cannot provide accurate values below the ozone peak (30 mb), so that information from ozonesondes and total ozone measurements must be used to provide complete vertical distributions.

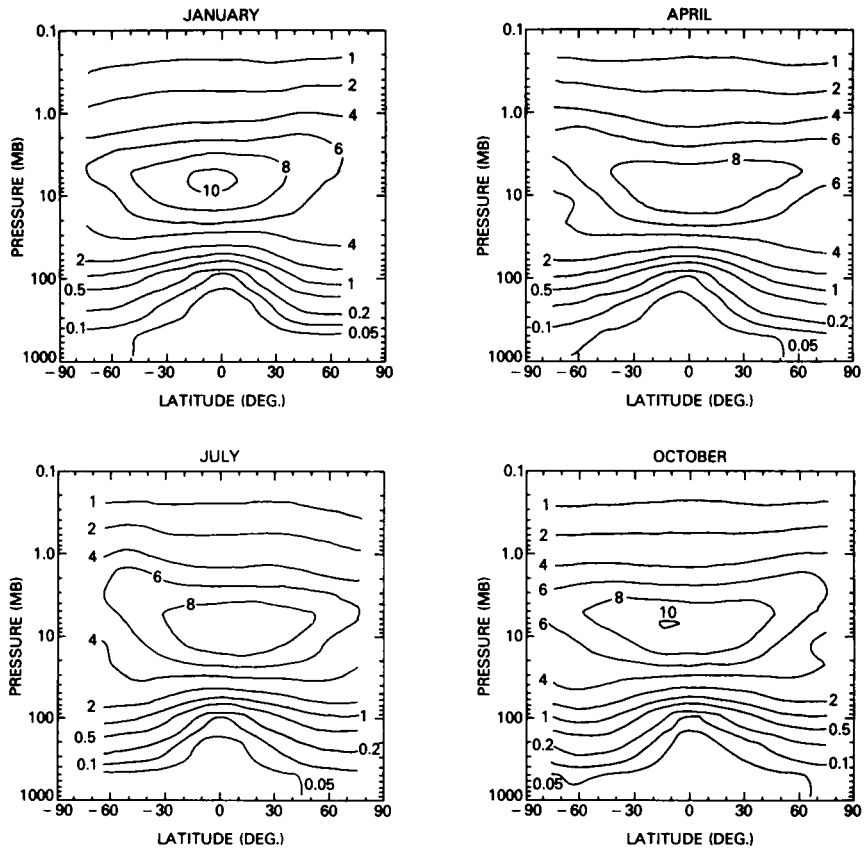

Fig. 10.4. Latitude-height sections of the ozone mixing ratio (ppmv) for January, April, July, and October 1979, as observed by the *Nimbus* 7 SBUV experiment. [After McPeters *et al.* (1984).]

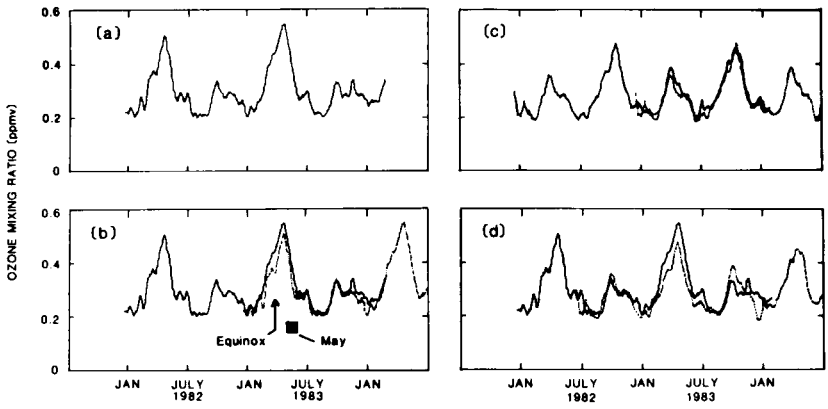

Fig. 10.5. Variation of the ozone mixing ratio at 0.01 mb during 1982–1983: (a) 45°N during 1982–1983; (b) 45°N with 1982 overlaid on 1983 (dotted); (c) 45°S with 1982 overlaid on 1983 (dotted); (d) 45°N (solid) with 45°S (dotted) overlaid with a 6-month time shift. Note the remarkable repeatability in the seasonal variation. [After Thomas *et al.* (1984).]

Figure 10.4 shows zonal-monthly mean sections of the ozone mixing ratio for January, April, July, and October 1979, based on the SBUV data from *Nimbus* 7. These indicate that in the photochemically controlled region of the middle and upper stratosphere the mixing ratio is a maximum in the equatorial region, but that in the transport-controlled region of the lower stratosphere the constant-mixing-ratio surfaces have poleward and downward slopes qualitatively consistent with transport by the Brewer–Dobson cell (cf. Fig. 9.4). These slopes are steepest in the spring hemisphere, reflecting the gradual buildup of ozone in the lower stratosphere during winter due to the rapid meridional transport and long photochemical timescale for the winter season.

In the extratropics the seasonal variation in the stratosphere is dominated by the annual harmonic; at most latitudes and heights there is a single maximum occurring in the spring. In the upper mesosphere, however, there is a dramatic semiannual cycle with a large peak in the spring, a secondary peak in the autumn, and minima at the solstices (Fig. 10.5). The ozone concentration at the spring equinox is more than twice that at the solstices. Such an extraordinary variability cannot be accounted for by photochemistry alone; it must reflect seasonal variability in dynamical processes that influence transport near the mesopause.

10.3 Elementary Aspects of Photochemical Modeling

The ozone climatology documented in the previous section cannot be understood without considering photochemical production and loss

processes, as well as the redistribution of ozone (and other trace gases involved in ozone chemistry) by atmospheric motions on all scales. The relative importance of photochemical and dynamical processes is highly dependent on altitude, latitude, and season. In this section we first indicate how the concept of chemical lifetime introduced in Section 9.2 can be employed to simplify the analysis of the behavior of ozone and other chemically active trace species. We then discuss the Chapman mechanism for formation of the ozone layer, which provides a simple illustration of the use of lifetime information, and hence provides a background for the modern theory of ozone photochemistry, which is briefly discussed in Section 10.4.

10.3.1 Some Scaling Considerations

The flux form of the tracer continuity equation for a chemically active tracer of volume mixing ratio χ can be written (see Appendix 10A) in the form

$$\chi_t + \rho_0^{-1} \nabla \cdot (\rho_0 \mathbf{u} \chi) = D + \rho_0^{-1}(T/T_s) N_a^{-1} M(P - L). \quad (10.3.1)$$

Here D designates diffusion by unresolved scales of motion, M is the molecular weight of air, N_a is Avogadro's number, T is temperature, T_s is a reference temperature (see Section 3.1.1), and P and L are the photochemical production and loss rates, respectively.

The importance of photochemistry in determining the distribution of any trace species can be assessed by comparing the magnitude of the production and loss terms with that of the flux divergence due to transport by motions of all scales. The simplest example is a tracer that is produced at the ground and photodissociated in the atmosphere (e.g., $CFCl_3$). For such a tracer, P vanishes and $L = J_A A$, where J_A designates the photodissociation rate coefficient (s^{-1}), and A designates the tracer concentration (molecules m^{-3}). Thus,

$$\left(\frac{\partial A}{\partial t}\right)_{\text{chemical}} \equiv P - L = -J_A A. \quad (10.3.2)$$

and the e-folding time scale for chemical decay of species A is simply $\tau_A = J_A^{-1}$. The relative roles of chemistry and transport in this situation can be assessed by comparing τ_A with the relevant dynamical time scale τ_d. The latter is given by the smaller of L_A/U or H_A/W, where L_A and H_A designate the horizontal and vertical scales of variation for the tracer mixing ratio and U and W are characteristic horizontal and vertical velocities. The dynamical timescale defined in this manner can vary enormously depending

on the spatial scale of the tracer mixing ratio variation. For example, in the lower stratosphere ozone has substantial variation on the synoptic scale ($L_A \approx 10^3$ km, $U \approx 10$ m s^{-1}), and the dynamical timescale for such variations is on the order of 1 day. On the other hand, for hemispheric-scale variations ($L_A \approx 10^4$ km) in the summer stratosphere (where eddy motions are very weak), the relevant velocity scale is the residual mean meridional velocity ($U \approx 10$ cm s^{-1}), and the dynamical timescale is in excess of 100 days. Thus, the relative importance of the dynamical and chemical terms in the tracer continuity equation depends crucially on the scale of variation considered.

In the case of hemispheric-scale transport, Fig. 9.2 indicates that for $CFCl_3$ $\tau_d \ll \tau_{CFCl_3}$ below 20 km, while $\tau_d \gg \tau_{CFCl_3}$ above about 30 km. Thus, since there is no chemical source for this trace gas in the stratosphere, the concentration decreases rapidly above 30 km. In the region 20 km $< z <$ 30 km, the distribution is determined by both transport and photochemical effects. Below 20 km, $CFCl_3$ is transported as a passive tracer.

An *e*-folding time scale for chemical decay can also be defined for molecules that are destroyed through bimolecular or termolecular reactions. Let A, B, and C stand for the concentrations of three different trace gases (molecules m^{-3}). If A and B react with reaction rate k_1 (m^3 molecule^{-1} s^{-1}) while A and C react in association with a third body of concentration M with reaction rate k_2(m^6 molecule^{-2} s^{-1}), then neglecting production processes,

$$\left(\frac{\partial A}{\partial t}\right)_{\text{chemical}} = -k_1 AB - k_2 ACM \equiv -A\tau_A^{-1}, \tag{10.3.3}$$

where $\tau_A \equiv (k_1 B + k_2 CM)^{-1}$, and it is here assumed that the concentrations B and C remain fixed on the timescale τ_A.

When the chemical time scale τ_A, defined on the basis of the *e*-folding rate for loss processes as in Eqs. (10.3.2) or (10.3.3), is short compared to the relevant dynamical timescale τ_d, then the loss must be approximately offset by photochemical production if the concentration A does not become negligible, in order that there be a balance in the continuity equation [Eq. (10.3.1)]. When the balance between production and loss is exact, the species is said to be in *photochemical equilibrium.* Such an equilibrium condition does not, of course, mean that transport is of no importance, since the concentrations of various species involved in the balance among production and loss processes may be strongly influenced by transport. As we shall see in the next subsection, at 30 km atomic oxygen, O, is in approximate photochemical equilibrium with O_3, but the concentration of total *odd oxygen*, defined as the sum of the concentrations of O and O_3 and designated by O_x($O_x = O + O_3$), is strongly influenced by transport processes.

10.3.2 *The Chapman Mechanism*

The Chapman reactions can be written in the following symbolic form:

$$(J_2) \quad O_2 + h\nu \rightarrow 2O, \tag{10.3.4a}$$

$$(k_2) \quad O + O_2 + M \rightarrow O_3 + M, \tag{10.3.4b}$$

$$(J_3) \quad O_3 + h\nu \rightarrow O + O_2, \tag{10.3.4c}$$

$$(k_3) \quad O + O_3 \rightarrow 2O_2. \tag{10.3.4d}$$

Here J_2 and J_3 are the rate coefficients for O_2 and O_3 photolysis, respectively; k_2 and k_3 are the reaction-rate coefficients for Eqs. (10.3.4b) and (10.3.4d). In the stratosphere, Eqs. (10.3.4b,c) are "fast" reactions, while Eqs. (10.3.4a,d) are 'slow." The net result of Eqs. (10.3.4a,b) is simply

$$3O_2 \rightarrow 2O_3.$$

Thus, these two reactions govern the production of O_3.

The reaction (10.3.4c) does not actually destroy O_3, since the atomic oxygen thus formed immediately reacts with O_2 to form ozone again, by Eq. (10.3.4b). This pair of fast reactions conserves O_x but interconverts O and O_3 and hence influences the partitioning of total odd oxygen between O and O_3: see Eq. (10.3.8).

In the original Chapman scheme, Eq. (10.3.4d) is the only reaction that serves to destroy ozone. It is now known that this reaction is much too slow to provide the rate of ozone destruction required to establish the observed ozone concentration in the stratosphere. A number of catalytic cycles involving "free radicals" (molecular fragments with unpaired electrons) of the nitrogen, chlorine, and hydrogen families are now believed to furnish the additional required sinks of O_3. These cycles are discussed in Section 10.4.

The net chemical tendencies for the O_3 and O concentrations as given by the Chapman reactions [Eqs. (10.3.4)] are

$$\left(\frac{\partial[O_3]}{\partial t}\right)_{\text{chemical}} = -J_3[O_3] - k_3[O][O_3] + k_2[O][O_2][M], \tag{10.3.5a}$$

and

$$\left(\frac{\partial[O]}{\partial t}\right)_{\text{chemical}} = -k_3[O][O_3] - k_2[O][O_2][M] + J_3[O_3] + 2J_2[O_2], \tag{10.3.5b}$$

where the concentrations are denoted by square brackets. At the 30-km level the timescales for chemical loss given by these reactions are (Brasseur and Solomon, 1984, pp. 205–206)

$$\tau_{O_3} = (J_3 + k_3[O])^{-1} = 2000 \quad \text{s}$$

and

$$\tau_O = (k_2[O_2][M] + k_3[O_3])^{-1} = 0.04 \quad \text{s}.$$

These are much shorter than the dynamical timescale, and can only be balanced by chemical production. Thus the net chemical sources, which determine the changes in mixing ratio following the motion, are given by very small differences between large terms of opposite sign. This is somewhat similar to the problem that arises in integration of the primitive equations in weather-prediction models. In that case the rate of change of momentum must be estimated from small differences between the pressure gradient force and the Coriolis force; small inaccuracies in either can produce huge errors in the computed tendency. As we saw in Chapter 3, this problem can be avoided in some situations by approximating the primitive equations by a prediction equation for a quasi-conserved quantity—quasi-geostrophic potential vorticity. Similarly, prediction of the evolution of the ozone field can be simplified by observing that the largest terms on the right of Eqs. (10.3.5) are those associated with the fast reactions [Eqs. (10.3.4b,c)], which represent cycling between O and O_3 but do not affect the total odd oxygen concentration. Thus, O_x should be more conservative than either O or O_3 alone.

Summing the two equations of Eqs. (10.3.5) we obtain

$$\left(\frac{\partial[O_x]}{\partial t}\right)_{\text{chemical}} = -2k_3[O][O_3] + 2J_2[O_2]. \tag{10.3.6}$$

In the stratosphere $[O] \ll [O_3]$, so that $[O_x] = [O] + [O_3] \approx [O_3]$ to a very good approximation. Thus, Eq. (10.3.6) provides a close approximation to the net source or sink for O_3 as given by the Chapman mechanism. The chemical loss timescale in Eq. (10.3.6) is

$$\tau_{O_x} = (2k_3[O])^{-1} \approx \text{weeks at 30 km},$$

which confirms that O_x is indeed far more conservative than O or O_3.

Noting that atomic oxygen has an extremely short chemical time constant, we can assume that [O] is in photochemical equilibrium with $[O_3]$ so that setting the left side to zero in Eq. (10.3.5b) gives

$$[O] = \frac{J_3[O_3] + 2J_2[O_2]}{k_3[O_3] + k_2[O_2][M]}. \tag{10.3.7}$$

In the stratosphere, $J_3[O_3] \gg J_2[O_2]$ and $k_2[O_2][M] \gg k_3[O_3]$, so that from Eq. (10.3.7),

$$[O]/[O_3] \approx J_3/(k_2[O_2][M]). \tag{10.3.8}$$

Thus, the $[O]/[O_3]$ ratio is closely determined by the fast reactions of Eqs. (10.3.4b,c).

In summary, for the Chapman chemistry, in the lower and middle stratosphere the ozone mixing ratio can be predicted from Eq. (10.3.1) with the chemical production and loss terms approximated by the right-hand side of Eq. (10.3.6), while the corresponding concentration of O can be computed at any instant from the equilibrium expression Eq. (10.3.7). In the upper stratosphere and mesosphere different balances hold (Brasseur and Solomon, 1984).

10.4 Photochemistry of Ozone: Catalytic Cycles

By substitution from Eq. (10.3.8), the loss rate for odd oxygen in Eq. (10.3.6) can be expressed in terms of the ozone concentration as

$$L = -2k_3[O_3]^2 J_3/(k_2[O_2][M]).$$

For observed ozone concentrations this rate is less than one-fourth of the ozone production rate in the stratosphere. The difference cannot be accounted for by transport processes; comparison of total global production and destruction rates indicates that ozone is formed 5 times faster than it is destroyed by the Chapman process.

The major loss of ozone is now known to occur through a number of catalytic reaction cycles, the simplest of which can be represented symbolically as follows:

$$X + O_3 \rightarrow XO + O_2 \tag{10.4.1a}$$

$$XO + O \rightarrow X + O_2 \tag{10.4.1b}$$

$$\text{Net:} \quad O + O_3 \rightarrow 2O_2$$

where X is a catalytic molecule that remains unchanged at the end of the cycle. The net effect of the catalytic cycles represented by Eqs. (10.4.1) is thus the same as that of Eq. (10.3.4d).

The efficacy of the cycle of Eqs. (10.4.1) is dependent on the speed of the slower of the two reactions. This is referred to as the *rate-limiting step.* The major free radicals in the stratosphere that can provide fast rates of reaction in *both* steps of Eqs. (10.4.1) are members of the odd hydrogen, odd nitrogen, and odd chlorine families (conventionally designated by HO_x,

NO_x, and Cl_x). Replacing the X in Eqs. (10.4.1) by OH, NO, or Cl yields a specific catalytic reaction cycle that is important in the stratosphere. In each of these cycles the rate coefficient for the rate-limiting step is typically several orders of magnitude larger than that for Eq. (10.3.4d).

The effectiveness of any such cycle is of course limited by the concentration of the catalyst as well as the reaction rate. In Fig. 10.6 the percentages of the odd oxygen production that are balanced by the HO_x, NO_x, and Cl_x cycles are shown as functions of altitude together with that of the Chapman mechanism. Because of the relatively large concentration of nitric oxide (NO), the NO_x cycle dominates throughout much of the stratosphere.

The concentrations of various catalytic free radicals depend on the processes that lead to their formation and removal. The source molecule for stratospheric NO_x is nitrous oxide (N_2O). Nitrous oxide, which is of biological origin, is well mixed in the troposphere with a volume mixing ratio of about 300 ppbv and is destroyed in the stratosphere primarily by ultraviolet photolysis to yield $N_2 + O$. A small fraction (1–2%) of the N_2O reacts with excited oxygen atoms in the stratosphere to produce NO. The main removal process for NO_x involves the reaction of nitrogen dioxide with the hydroxyl radical:

$$HO + NO_2 + M \rightarrow HNO_3 + M. \tag{10.4.2}$$

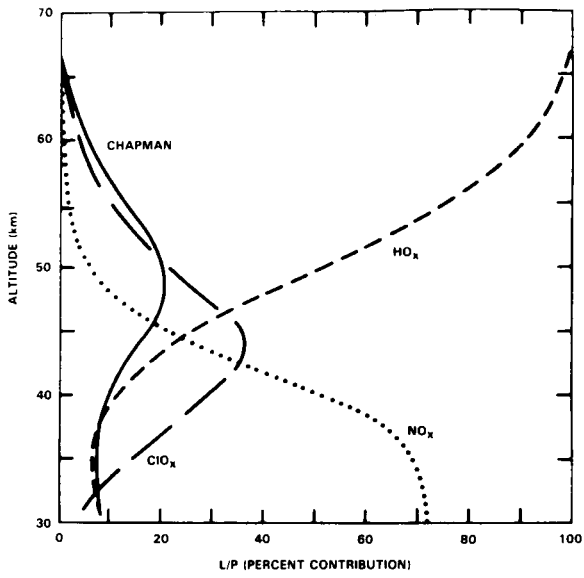

Fig. 10.6. Ratio (in percent) of the odd oxygen loss rate (L) due to the Chapman HO_x, NO_x, and Cl_x mechanisms to the odd oxygen production rate (P) based on midlatitude diurnally averaged conditions. [From Watson *et al.* (1986), with permission.]

The nitric acid (HNO_3) formed in this reaction has a fairly long chemical lifetime and is removed by transport into the troposphere, where it dissolves in water droplets and is rained out.

The hydroxyl radical (OH) participates in many important chemical reactions in the troposphere and stratosphere. OH is formed primarily through the reactions of $O(^1D)$ with water vapor and methane. An important path for removal is by coupling to the NO_x cycle through the reaction of Eq. (10.4.2).

The source for chlorine in the natural stratosphere is the upward transport of methyl chloride (CH_3Cl), whose main source is the world ocean. Methyl chloride reacts with the OH radical in the atmosphere to provide free chlorine for participation in the Cl_x cycles. In addition, methyl chloride is photolyzed above 30 km; this process also forms Cl_x.

Because it is chemically attacked by the OH radical, which is present in the troposphere as well as the stratosphere, methyl chloride has a relatively short tropospheric lifetime; most of it is destroyed before it can reach the stratosphere. The same is not, however, true of the chlorofluoromethanes ($CFCl_3$, and CF_2Cl_2). These synthetic species are almost completely inert in the troposphere but are photolyzed in the stratosphere, where they now provide the predominant source of chlorine. The atmospheric concentration of the chlorofluoromethanes is increasing at a rate of about 5% per year. Thus, they potentially could cause a substantial perturbation to the natural balance of the ozone layer.

The principal sink for stratospheric chlorine is the reaction of chlorine with methane to form hydrochloric acid:

$$Cl + CH_4 \rightarrow HCl + CH_3.$$

HCl is relatively long-lived in the stratosphere and, like HNO_3, is transported to the troposphere and rained out.

Chemical models of the ozone layer must account for the sources and sinks of the catalytic molecules, as well as the partitioning that occurs due to the many reactions among the various species. The rates of ozone destruction by the HO_x, NO_x, and Cl_x families of reactions cannot simply be added together to give the total catalytic destruction rate. Because of the coupling among the catalytic cycles, the rate of destruction for one set of reactions may depend on the concentration of another catalytic species. In addition to the cycles considered here, which involve atomic oxygen and thus are primarily important only in the middle and upper stratosphere where atomic oxygen is present in significant amounts, there are cycles in which ozone replaces atomic oxygen as a reactant. There are also null cycles that involve interconversion among the reacting species, and reactions that sequester free radicals in temporary reservoir species so that they are

unavailable for participation in ozone-destroying cycles. ($ClONO_2$ is a notable example of such a temporary reservoir.) There are even some chemical cycles that actually produce ozone in the lower stratosphere and troposphere. Detailed models of the ozone layer may involve more than 100 chemical and photochemical equations. Only about a dozen species or families of species are directly affected by transport processes. But others are indirectly affected, since their photochemical equilibrium states depend on the concentrations of species that are themselves partly transport controlled.

10.5 Models of the Natural and Perturbed Ozone Layer

Realization that human activities might lead to depletion of the ozone layer has in recent years provided motivation for extensive attempts to model the natural and perturbed ozone distribution. As indicated in the last section, when the catalytic ozone destruction cycles involving the HO_x, NO_x, and Cl_x families and the coupling among these are included, the computation of photochemical production and loss of ozone becomes quite complicated. Partly because of the resulting enormous computational demands of three-dimensional modeling, most simulations of the ozone layer have been based on either one-dimensional or two-dimensional models. The former can only provide information on the horizontally and annually averaged vertical profile, while the latter can include latitudinal and seasonal dependence.

One-dimensional models can only account for transport in a very crude fashion by parameterizing all transport effects in terms of vertical diffusion. Such models can, however, include rather complete representation of photochemical processes and can be integrated for long periods of simulated time with rather modest computational resources. Two-dimensional models can in principle simulate the effects of meridional and vertical transport as well as meridional variations in photochemistry. The fidelity of such simulations depends, of course, on the accuracy with which the zonally averaged eddy transports can be represented.

10.5.1 Two-Dimensional Modeling of the Natural Ozone Layer

A number of two-dimensional models of the ozone layer have been formulated over the past two decades. The earliest of these were based on the conventional Eulerian-mean formulation. In most cases such models employed the tracer continuity equation [Eq. (9.7.1)] with a specified Eulerian-mean meridional circulation ($\bar{v}$, $\bar{w}$) estimated with the aid of

observational data, and an empirically determined symmetric diffusion tensor.

In this formulation there should be a large degree of cancellation between two poorly known properties, the "eddy" and the "mean" transport. For this reason the traditional Eulerian-mean approach has been abandoned by most modelers. Currently, an approximate TEM formulation [Eq. (9.4.7) with the effective transport velocity approximated by the residual circulation] or an isentropic formulation [see Eq. (9.4.27)] is favored. Either of these tends to reduce the cancellation between "eddy" and "mean" transports that occurs in the conventional Eulerian mean formulation.

A further important distinction among the two-dimensional models is between those in which the meridional circulation is specified and those in which it is computed self-consistently from the complete zonally averaged equations [i.e., Eqs. (3.5.2) in the case of the TEM formulation]. In the former case it is usual to assume that the residual circulation is approximated by the diabatic circulation and to use theoretically derived estimates of the diabatic heating rate, using observed temperatures, as a function of latitude, height, and season to obtain the $(\bar{v}^*, \bar{w}^*)$ field.

Models in which the zonal mean dynamical equations are solved must, of course, employ parameterizations of the eddy forcing in the zonal mean momentum and thermodynamic equations. It is also necessary to solve for the zonal mean diabatic heating corresponding to the seasonally varying temperature and ozone distributions computed in the model. An example of this type is the model of Garcia and Solomon (1983), in which the parameterized planetary waves are assumed to be steady, linear, and adiabatic so that their EP flux divergence vanishes. Thus, the model does not include parameterized meridional mixing by transient planetary waves. It does include weak meridional and vertical eddy diffusion terms in the thermodynamic equation and tracer continuity equation to parameterize the effects of mixing by small-scale disturbances. The momentum budget is approximately accounted for by a balance between the Coriolis torque of the residual meridional motion and a strongly altitude-dependent Rayleigh friction that is intended to model gravity-wave drag. The mean meridional mass stream function for the residual circulation given by this model is shown in Fig. 10.7. The corresponding Northern-Hemisphere winter solstice ozone distribution is shown in Fig. 10.8; this may be compared with the observed distribution of Fig. 10.4. Clearly this type of model, in which transport is dominated by the advection due to the residual circulation, does a surprisingly good job of modeling the distribution of ozone in the meridional plane.

The TEM version of the tracer continuity equation used by Garcia and Solomon (1983) does not completely neglect meridional transport by

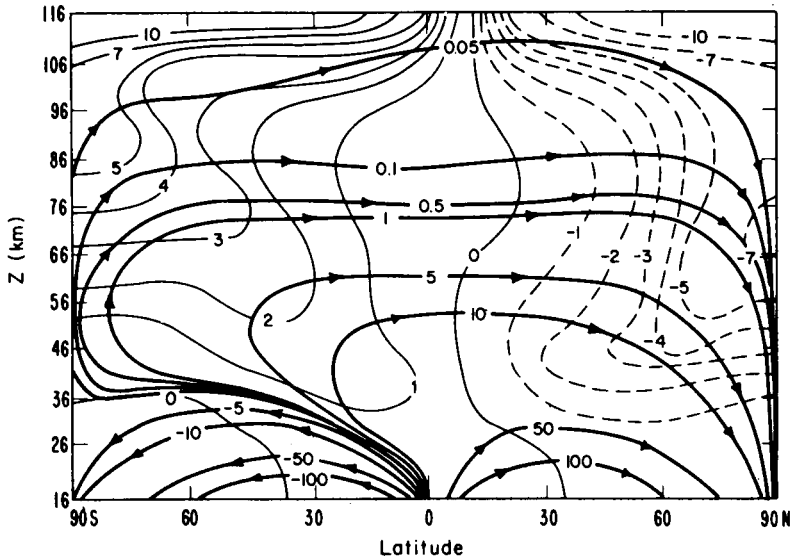

Fig. 10.7. Mass stream function for the residual meridional circulation (kg m^{-1} s^{-1}) shown in heavy solid lines and the diabatic heating distribution (light solid and dashed lines; K day^{-1}) for Northern-Hemisphere solstice conditions as computed in a two-dimensional model. [After Garcia and Solomon (1983).]

planetary waves. Even though transient eddy effects are ignored, the model does include a treatment of the flux divergence due to eddy chemical dissipation by steady planetary waves. This is modeled in a manner similar to the weak linear relaxation treatment of Section 9.4.1. Garcia and Solomon also include effects of temperature-dependent reaction rates in the photochemistry of ozone. Thus, they let

$$S' = -a\chi' - b\theta'$$

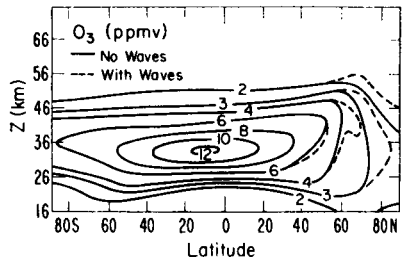

Fig. 10.8. Ozone mixing ratio computed in the two-dimensional model whose residual meridional circulation was indicated in Fig. 10.7. The dashed contours show the effects of transport due to chemical dissipation in steady planetary waves (see text for details). [After Garcia and Solomon (1983).]

where $b = \bar{\chi}\,\partial a/\partial\bar{\theta}$ (units of $K^{-1}\,s^{-1}$). In that case it may be verified by the methods of Section 9.4.1 that the modified Eulerian source of Eq. (9.4.10) must have an additional term of the form

$$\rho_0^{-1}\,\nabla\cdot(\rho_0\mathbf{K}^{(T)}\cdot\nabla\bar{\theta}) \tag{10.5.1}$$

where $\mathbf{K}^{(T)} \equiv ba^{-1}\mathbf{K}^{(c)}$. Thus, for ozone the source modification (sometimes referred to as the "chemical eddy" effect) involves two flux divergence terms: the first has the flux proportional to the zonal-mean tracer mixing ratio gradient; the second has the flux proportional to the zonal-mean potential temperature gradient. The modification to the Northern-Hemisphere winter solstice ozone distribution due to the chemical eddy effect is shown in Fig. 10.8. Only at relatively high latitudes, where the stationary planetary wave amplitudes are large, is the planetary-wave chemical eddy effect significant.

10.5.2 Modeling Mesospheric Ozone

In Section 10.2 we pointed out that observations indicate that near the mesopause the seasonal variation of ozone is characterized by a strong maximum at the spring equinox, a secondary maximum at the autumn equinox, and minimum at the solstices. If ozone at this level were under photochemical control, the maximum would occur at the summer solstice, since the temperature-dependent reactions that destroy ozone would be slowest in the cold summer mesosphere and the production rate would be a maximum. Thus, the observed distribution must be dynamically controlled.

As discussed in Section 4.6.2, gravity wave breaking is thought to generate a strong zonal drag force and large vertical diffusion in the mesopause region. Although little is known about the climatology of gravity-wave sources, it is clear that gravity-wave transmissivity must depend on the mean wind distribution in the stratosphere and mesosphere. During the winter season, when stationary gravity waves can propagate through the bulk of the middle atmosphere, strong gravity wave breaking is expected to occur in the upper mesosphere. During the summer season, when a zero wind line in the lower stratosphere separates tropospheric westerlies from stratospheric easterlies, the transmission of low-phase-speed wave modes will be inhibited; only waves with westerly phase speeds great enough to escape the troposphere will be able to penetrate to the mesopause. Since such waves are expected to have lower amplitudes than the low-phase-speed waves, the wave-breaking region will be higher than in the winter. During the equinoctial seasons the zonal winds tend to be weak westerly in the stratosphere and weak easterly in the mesosphere. Under these conditions only the high-phase-speed "tail" of the gravity-wave spectrum can propagate

to the mesopause region; wave breaking and turbulence should then be much reduced.

Thomas *et al.* (1984) argued that the seasonal variability in the vertical diffusion at the mesopause generated by breaking gravity waves could, by altering the rate of vertical tracer transport, account for the observed equinoctial peaks in the ozone distribution near the mesopause. Reduced vertical transport at the equinox should have two important effects. First, the downward flux of atomic oxygen below the 80-km level would be reduced. This fact, combined with the more or less steady downward diffusion from the thermosphere, would lead to a buildup of atomic oxygen near the mesopause. Second, there would be a reduced upward transport of water vapor from the lower mesosphere. The former effect would tend to increase the rate of ozone formation; the latter would tend to reduce the amount of OH available for catalytic destruction of ozone.

In Fig. 10.9 the equinox to solstice ozone ratio observed by the SME satellite is compared with results from a two-dimensional model that includes the simple parameterization of gravity wave breaking and diffusion discussed in Section 4.6.2. The extratropical equinoctial ozone maximum is well simulated, suggesting that seasonal variation of turbulent diffusion by breaking gravity waves is the correct explanation for the equinoctial ozone maximum.

10.5.3 One-Dimensional Models of Ozone Perturbations

The one-dimensional model remains a popular tool for studying the response of the ozone layer to various postulated secular changes in trace gases. In most one-dimensional models the tracer concentrations are carried as independent variables. The concentration (number density) of the ith species, n_i, is then predicted from an equation of the form

$$\frac{\partial n_i}{\partial t} = \frac{\partial}{\partial z^*}\left[\hat{K}_{zz}\rho\frac{\partial}{\partial z^*}(n_i/\rho)\right] + P_i - L_i \tag{10.5.2}$$

where P_i and L_i are the photochemical production and loss rates for the ith species, $\hat{K}_{zz}$ is the vertical diffusion coefficient, z^* designates the geometric height, and ρ is the air density.

In most one-dimensional formulations, $\hat{K}_{zz}$ is determined empirically so that Eq. (10.5.2) provides the steady-state observed distribution of CH_4 at 30°N latitude. As discussed in Section 9.7.3, the diffusion coefficient in a one-dimensional model should not be the same for every species, but should be smaller for those species with shorter lifetimes (see Fig. 9.17). Most formulations to date have, however, employed the same value of $\hat{K}_{zz}$ for all species.

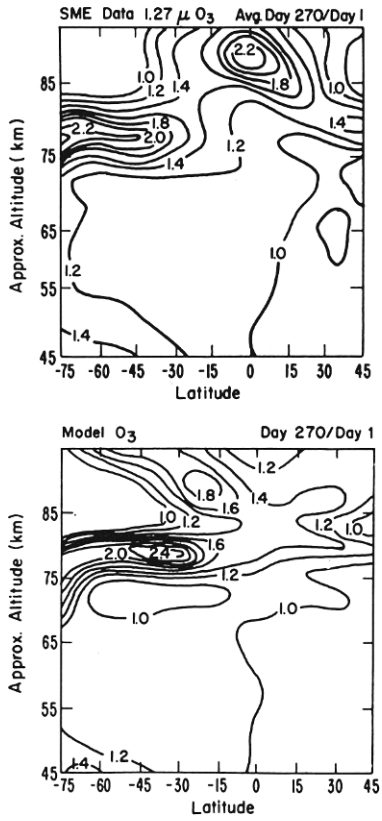

Fig. 10.9. The ratio of O_3 concentration at the Southern-Hemisphere spring equinox to that at the southern summer solstice as measured by the SME satellite (upper) and simulated in a two-dimensional model that includes parameterized gravity wave diffusion (lower; see text for details). [After Garcia and Solomon (1985).]

The concentrations governed by Eq. (10.5.2) should be interpreted as global averages at constant height. In most cases global data are not available for chemical tracers, and it is not possible to compute global means of the production and loss terms without knowledge of the meridional distribution of the tracers. Thus, one-dimensional models have often been regarded as providing vertical profiles at 30°N, a location for which there is a considerable data base, and production and loss terms are computed for annual mean conditions at 30° latitude.

The major use of one-dimensional photochemical models is to provide information on possible perturbations of the ozone layer due to trends in various trace gases that participate in chemical reactions that may affect ozone. The gases that are currently deemed to pose the greatest threat to

the ozone layer are the synthetic chlorofluoromethanes, $CFCl_3$ and CF_2Cl_2, which are widely used as coolants in refrigeration, in industrial foam blowing, and as aerosol propellants. Most of these gases are eventually released into the troposphere and transported into the stratosphere, where they are photolyzed to produce free chlorine, which then reacts catalytically to destroy ozone. Although, as mentioned in Section 10.4, chlorine chemistry is not the major source for ozone destruction in the natural stratosphere, the increase of chlorine in the atmosphere due to the release of $CFCl_3$ and CF_2Cl_2 is several percent per year; already chlorine of anthropogenic origin constitutes the major portion of the total chlorine content of the stratosphere. Estimates of the eventual decrease in ozone abundance that would result

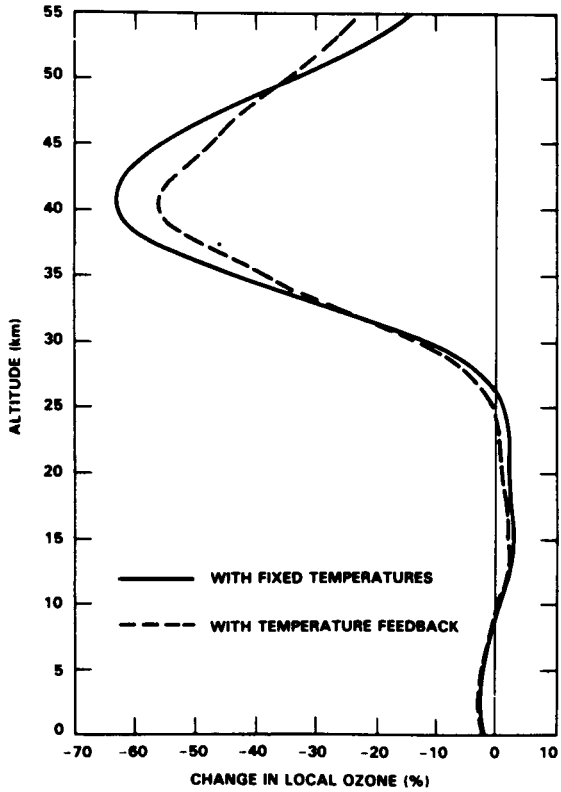

Fig. 10.10. One-dimensional model predictions (Lawrence Livermore National Laboratory model) of the percentage change in ozone concentration at steady state as a function of height for continuous release of chlorofluoromethanes at 1980 rates, relative to the atmosphere with no chlorofluoromethanes. [From Watson *et al.* (1986).]

from release of chlorine at a constant rate indefinitely into the future have varied markedly as information on reaction rates has been refined. Current estimates suggest that there should be only a few percent depletion in the ozone column at steady state for release at the 1980 rate. This steady state would not be reached, however, until late in the next century.

The predicted small net change in the ozone column results from a "self-healing" effect in which large reductions in the upper and middle stratosphere induced by the catalytic chlorine destruction reactions are to a large extent cancelled by increases at the lower levels (Fig. 10.10). The predicted increase in the lower stratosphere is due both to increased production associated with the greater penetration of solar ultraviolet radiation and to formation of the "reservoir" species chlorine nitrate, which reduces the amount of Cl and NO available to participate in the catalytic ozone destruction cycles. For current release rates of chlorofluoromethanes, this process is very effective in limiting the total change in column abundance of ozone. But if the rate of chlorofluoromethane release were to continue to increase, eventually all of the NO_x in the lower stratosphere would be transferred to the chlorine nitrate reservoir, and further increases of chlorine would then be expected to cause rapid decreases in ozone.

Although most perturbation studies have been limited to examining the effects of changes in a single radiatively or chemically important species, the effects of individual perturbing gases should not be considered in isolation, since significant coupling effects might occur. Some of these are briefly discussed in Chapter 12.

Appendix 10A The Continuity Equation for Chemical Species

In atmospheric chemistry the tracer continuity equation is usually expressed in terms of the number density n (molecules m^{-3}) of the tracer. It takes the form [e.g., Brasseur and Solomon (1984), Eq. (3.36)]

$$\frac{\partial n}{\partial t} + \nabla^* \cdot (n\mathbf{u}^*) = P - L, \tag{10A.1}$$

when P and L are the "production" and "loss" terms (molecules $m^{-3}\,s^{-1}$) and asterisks indicate the use of geometric-height (z^*) coordinates, rather than the log-pressure (z) coordinates that are mostly adopted in this book. Now by Eqs. (1.3.1) and (1.3.3a),

$$n = (N_a M^{-1})\rho\chi, \tag{10A.2}$$

where ρ is the air density, χ is the volume mixing ratio, M is the molecular weight of air, and N_a is Avogadro's number. On substituting Eq. (10A.2)

into Eq. (10A.1) and using the mass continuity equation in z^* coordinates,

$$\frac{\partial \rho}{\partial t} + \nabla^* \cdot (\rho \mathbf{u}^*) = 0, \tag{10A.3}$$

we obtain

$$\frac{D\chi}{Dt} \equiv \frac{\partial \chi}{\partial t} + \mathbf{u}^* \cdot \nabla^* \chi = \rho^{-1} N_a^{-1} M(P - L). \tag{10A.4}$$

Note that derivatives with respect to x, y, and t are here taken at constant z^*, not at constant z. However, D/Dt is a coordinate-independent operator and can alternatively be expressed in its z-coordinate form (see Section 3.1.1). Using the ideal gas law [Eq. (1.1.1)] and the expression $\rho_0(z) = p/RT_s$ (Section 3.1.1), we can thus write Eq. (10A.4) in the z-coordinate form

$$\frac{D\chi}{Dt} \equiv \chi_t + \mathbf{u} \cdot \nabla \chi = \rho_0^{-1}(T/T_s) N_a^{-1} M(P - L) \equiv S, \tag{10A.5}$$

where x, y, t derivatives are now taken at constant z [cf. Eq. (9.4.1)]. An alternative z-coordinate form, derived from Eqs. (10A.5) and (3.1.3d), is

$$(\rho_0 \chi)_t + \nabla \cdot (\rho_0 \chi \mathbf{u}) = (T/T_s) N_a^{-1} M(P - L) = \rho_0 S \tag{10A.6}$$

[cf. Eq. (9.4.2)]. In practice, a further term representing small-scale diffusion should also be added to the right-hand side of Eq. (10A.6): see Eq. (10.3.1).

References

10.2. London (1985) presents an excellent review of observational studies of the climatological mean and variability of atmospheric ozone, with an emphasis on ground-based observations. His paper contains an extensive bibliography.

10.3. The concept of chemical time scales is developed thoroughly in Brasseur and Solomon (1984). They also provide a general discussion of the chemistry of the middle atmosphere.

10.4. The fundamentals of ozone photochemistry are presented clearly in Wayne (1985). Other treatments of the subject include Thrush (1980) and Whitten and Prasad (1985).

10.5. Watson *et al.* (1986) present a summary of model calculations of the perturbed ozone layer and also review many aspects of the radiative, dynamical, and chemical processes that are of importance in the stratosphere. Their work is essentially a summary of the detailed presentation given in WMO (1986).